

## Laboratory and Testbeam Results on 3D Detectors

---

**Celeste Fleta\***, Giulio Pellegrini, Manuel Lozano

*Instituto de Microelectrónica de Barcelona IMB-CNM (CSIC), 08193 Bellaterra, Barcelona, Spain.*

*E-mail: Celeste.Fleta@imb-cnm.csic.es*

**Richard Bates, Aaron Mac Raighne, Chris Parkes, Graeme Stewart**

*Department of Physics and Astronomy, University of Glasgow, Glasgow G12 8QQ, UK.*

**Michael Köhler, Ulrich Parzefall, Liv Wiik**

*Institute of Physics, University of Freiburg, Hermann-Herder-Str. 3, 79104 Freiburg, Germany.*

**Eva N. Gimenez, Julien Marchal, Nicola Tartoni**

*Diamond Light Source, Harwell Science and Innovation Campus, Didcot, Oxfordshire OX11 0DE, UK.*

This paper reports on recent test beam and laboratory results performed on 3D strip and pixel detectors. The devices were produced using a special double-sided 3D technology aimed to simplify the fabrication process, where the columnar electrodes etched into the silicon do not pass through the full substrate thickness.

Double-sided 3D n-in-p strip detectors show good electrical and charge collection characteristics after heavy irradiation up to  $2 \times 10^{16} n_{eq}/cm^2$ . An effect of charge multiplication is observed at high bias voltages, both in laboratory tests with radioactive source and in beam tests with pions. This multiplication effect is beneficial for the signal-to-noise ratio for moderate voltages and values  $> 40$  can be achieved.

The detection efficiency and charge sharing properties of the 3D structure have been investigated in Medipix2 pixel detectors with micro-focus synchrotron X-rays and pion beams and compared to that of the standard planar technology. There is a drop in the detection efficiency over the pixel of the 3D sensors due to the central electrodes, however the corner electrodes do not represent a significant degradation of the efficiency compared to that of the planar devices. The 3D sensors show a considerably reduced charge sharing compared to planar detectors that makes them very interesting for imaging applications.

*19th International Workshop on Vertex Detectors*

*June 6 -11 2010*

*Loch Lomond, Scotland, UK*

---

\*Speaker.

## 1. 3D detectors

3D silicon radiation detectors, first proposed by Sherwood Parker *et al.* [1], consist of a three-dimensional array of p and n electrodes that penetrate into the detector bulk perpendicular to the surface. In traditional planar detectors the electrodes are implanted in the top and bottom surfaces of the wafer so the maximum drift and depletion distances are set by the wafer thickness. By contrast, 3D detectors deplete laterally, so these distances are given by the inter-column spacing that can be much smaller than the wafer thickness. The reduced electrode distance results in high electric fields and high drift velocities with relatively low bias voltages that reduce the probability of trapping and make the devices radiation hard. Results of measurements of heavily irradiated detectors that demonstrate the advantage of the 3D design for harsh radiation environments will be presented in section 3.

3D detectors are also interesting for imaging applications because the electric field pattern causes the charge carriers to drift horizontally far from the pixel boundaries resulting in a reduced charge sharing, as will be shown in section 4.1. Thanks to this self-shielding effect of the electric field, 3D sensors can be diced very close to the active area and offer the possibility of tiling a large number of small detectors for large modular detector designs. Furthermore, it is possible to use the same fabrication tools used to produce the electrodes to add an "active edge" electrode to the 3D sensor to extend the sensitive area to within  $10\mu\text{m}$  of the physical edge [2].

All these advantages of 3D sensors over standard planar sensors have the cost of a higher technological difficulty as the fabrication of the 3D electrodes involves several complex steps (attachment and removal of a sacrificial support wafer, DRIE micromachining of the columns, doping and filling of the electrodes) that need to be carefully optimized and increase the fabrication cost [3]. However, there is a growing interest in the possibilities of 3D detectors and several research groups have recently developed their own 3D technologies with promising prospects for a small-medium scale production [4–8].

This paper presents experimental results of 3D silicon sensors fabricated with a special double-sided 3D technology which aims to simplify the fabrication process. The device design and the fabrication technology are described in section 2. Section 3 focuses on results from double-sided 3D strip detectors fabricated on a p-type substrate and includes irradiation and annealing studies, charge collection laboratory tests with radioactive sources and beam test measurements after heavy irradiation. Finally, section 4 presents detection efficiency and charge sharing results from double-sided 3D pixel detectors with the Medipix2 geometry, comparing their performance to that of standard planar sensors.

## 2. The double-sided 3D design

IMB-CNM (Barcelona, Spain) uses a double-sided technique for the fabrication of 3D detectors where the columnar electrodes are etched from opposite sides of the wafer and do not pass through the full thickness [7]. This simplifies the fabrication process and makes the wafers more mechanically resistant, which improves the production yield and reduces the cost. Fondazione Bruno Kessler (FBK) of Trento, Italy, also have produced double-sided 3D detectors with a slightly different design [8].

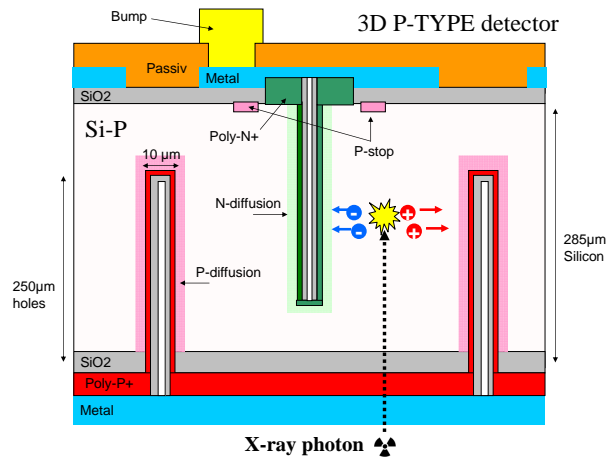


**Figure 1:** Structure of a double-sided 3D detector with p-type substrate.

Simulations of the double-sided structure [9] show that in the region where the columns overlap the electrostatic behaviour of the detector matches that of a full 3D detector. The volume near the front and back of the detector has a lower electric field, so the charge produced in these regions is collected less quickly. After irradiation, the collection efficiency falls more quickly in the double-sided device than in the full 3D due to incomplete depletion and greater trapping of carriers in the low field regions. However, the irradiated double-sided 3D detector still is expected to have much higher charge collection than the equivalent planar sensor [10].

The detectors used in this study were fabricated at the clean room of IMB-CNM on high resistivity, 4" wafers from Topsil, with orientation  $\langle 100 \rangle$  and thickness  $285 \pm 15 \mu\text{m}$ . The deep silicon etch was done with an Alcatel 601E machine using the Bosch process to produce holes with  $10 \mu\text{m}$  diameter and  $250 \mu\text{m}$  deep. Next, the columns were partially filled with a  $3 \mu\text{m}$  polysilicon layer and doped with boron ( $\text{p}^+$ ) or phosphorous ( $\text{n}^+$ ). Finally, the electrodes were passivated with an oxide layer. Details of the fabrication technology can be found in [7].

The structure of a double-sided 3D detector fabricated on p-type silicon is shown in Figure 1. The phosphorus-doped  $\text{n}^+$  columns at the front surface are the electron-collecting electrodes. The boron-doped  $\text{p}^+$  columns extending from the back surface are connected together with polysilicon and metal layers and are used for biasing. In an n-type, hole-collecting detector the column types are reversed. This structure is fully compatible with standard pixel read out electronics as the high voltage can be applied on the back of the pixels like in a planar device.

### 3. Results from 3D strip detectors

This section presents test results from double-sided 3D strip detectors fabricated on a p-type substrate. The detectors have 50 DC-coupled strips, each one with 50  $\text{n}^+$  columns separated  $80 \mu\text{m}$ . There is a common p-stop surrounding the sensor area and individual p-stops around each electrode to provide surface isolation. A 3D guard ring of  $\text{n}^+$  columns surrounds the device.

These 3D strip detectors show two stages in the depletion process as corresponds to their double-sided structure [9]. First, the depletion region grows horizontally and vertically outwards from the  $n^+$  columns so that the region where the columns overlap is fully depleted at about 4V. In a second stage, the depletion region continues to grow vertically until the detector volume is fully depleted at about 40V.

In the current-voltage tests of the fabricated p-type sensors, only 2 of 19 (11%) show electrical breakdown at less than 5V, probably due to defects produced by the deep silicon etching of the holes. The others have good characteristics up to at least 200V, well beyond full depletion. The leakage current is between 40–120pA/column at 20°C, very stable after full depletion.

The capacitance between one readout strip and the bias columns, which dominates the total capacitance, is about 5pF/strip (12.5pF/cm). It was measured at 20°C with an AC signal of 10kHz, with the two neighbours at the same potential as the central strip. The interstrip capacitance measured between one strip and its two neighbours, with the guard ring grounded and the backside biased for full depletion, is 1.5pF/strip (3.7pF/cm).

### 3.1 Irradiation and annealing studies of strip detectors

The 3D strip detectors were irradiated at the Karlsruhe Institute of Technology with 25MeV protons to equivalent doses between  $5 \times 10^{14}$  and  $2 \times 10^{16} n_{eq}/cm^2$  (a hardness factor of 1.85 was used to convert the proton fluences to 1MeV neutron equivalent fluences.) The sensors were irradiated cold and without bias and immediately after the irradiation were stored at  $-20^\circ\text{C}$  or less to prevent unintentional annealing effects.

The electrical characteristics of the irradiated sensors were measured in a probe station at a temperature of  $-10^\circ\text{C}$ . As expected the depletion voltage increases after irradiation as the effective doping concentration increases: the lateral depletion voltage extracted from the C-V plots is 145V for a fluence of  $10^{16} n_{eq}/cm^2$  (this value is still lower than in the equivalent planar sensor thanks to the reduced electrode spacing.) Additionally the interstrip resistance decreases with the irradiation dose due to the build-up of a negative charge in the silicon-oxide interface. The resistance measured for a sensor irradiated to  $10^{16} n_{eq}/cm^2$  is 100M $\Omega$  at 150V (it was of the order of 100G $\Omega$  before irradiation), which shows that the p-stop isolation works well even for these high radiation doses.

The annealing effect on the electrical characteristics was studied with a 3D strip detector irradiated to  $10^{16} n_{eq}/cm^2$ . The sensor was heated in timed steps at 80°C that means an acceleration factor of 7400 for the reverse annealing with respect to room temperature. The current-voltage curves of the sensor as a function of the annealing time are shown in Figure 2. Two competing effects can be seen in the plots: for low voltages there is the expected reduction in the leakage current as the annealing time increases [11]. However, for voltages higher than 200V this trend is reversed and the current starts to increase for longer annealing times. This behaviour suggests there is an avalanche multiplication effect of the thermally-generated carriers for high values of the electric field in the sensor.

### 3.2 Charge collection tests of strip detectors with radioactive source

Collection tests of the double-sided strip detectors with a Sr-90 radioactive source were performed at the University of Glasgow [12]. The detectors were readout with the Alibava data acquisition system [13], based on the Beetle chip developed for the LHCb experiment, with a scintillator

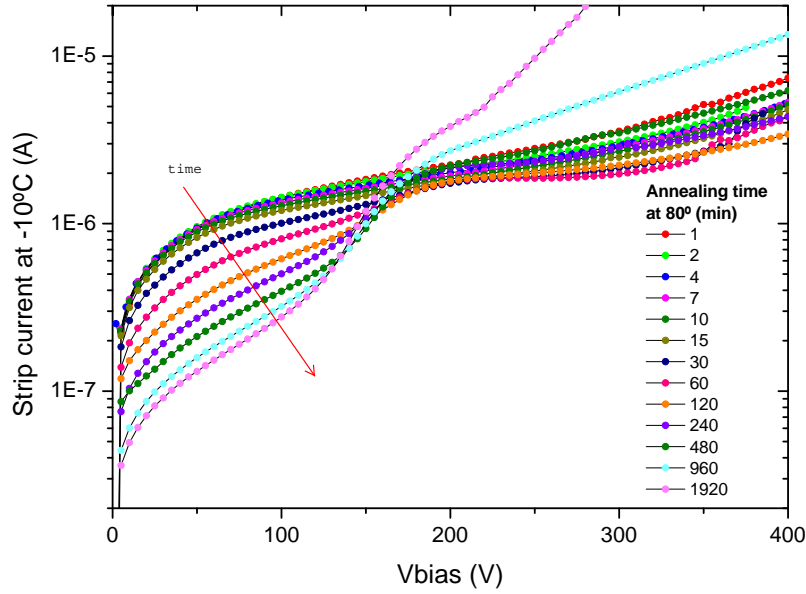


**Figure 2:** Annealing of the I-V characteristics of a double-sided 3D p-type sensor irradiated to  $10^{16}n_{eq}/cm^2$ .

located behind the device under test for triggering. The collected charge (Landau most probable value) as a function of the bias voltage was measured for the full range of irradiation doses. An unirradiated planar strip detector was used to calibrate the system, with the plateau value of the collected charge taken as full collection.

The non-irradiated 3D devices show 100% collection efficiency ( $22.8ke^-$ ) at full depletion. Only moderate bias voltages, 150V, are necessary for full charge collection for fluences up to  $10^{15}n_{eq}/cm^2$ . Higher radiation doses reduce the collection efficiency but for  $10^{16}n_{eq}/cm^2$  the collected charge at 150V is close to 44%, 10000 electrons ( $10^{16}n_{eq}/cm^2$  is the fluence expected for the sLHC lifetime at a radius of 5cm from the interaction point.) To compare, a  $300\mu m$  thick p-type planar sensor irradiated to the same fluence of 25MeV protons has  $\approx 25\%$  collection efficiency at 900V bias [14]. These measurements demonstrate the advantage of the 3D detectors over the planar design for high radiation environments, as their higher electric field for a given sensor bias results in a higher charge drift velocity and lower trapping.

The performance of the irradiated sensors at high bias voltages was also studied. The devices were biased to the maximum voltage allowed before they suffered electrical breakdown or the noise or the current became too high, typically in the 250–350V range. The results are shown in Figure 3. A strong effect of charge multiplication can be seen in all devices: the charge collection efficiency is higher than 100% for irradiation doses lower than  $2 \times 10^{15}n_{eq}/cm^2$ , close to 100% for  $10^{16}n_{eq}/cm^2$  at 350V and 50% for  $2 \times 10^{16}n_{eq}/cm^2$  at 300V. This enhanced charge collection at high irradiation doses had previously been observed in double-sided 3D detectors fabricated by FBK and irradiated with 25MeV protons up to  $2 \times 10^{15}n_{eq}/cm^2$  [15], and also in standard and thin planar detectors at higher bias voltages [16–18]. The effect is likely due to impact ionisation of the charge carriers in high electric field regions, although it is not well understood yet.

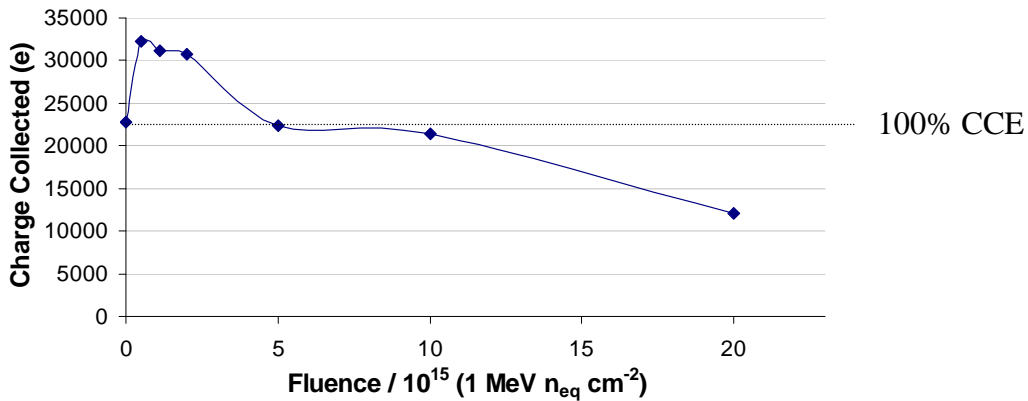


**Figure 3:** Charge collected by the irradiated strip detectors at high bias (250–350V).

### 3.3 Pion beam tests of strip detectors

The 3D strip detectors were tested in realistic working conditions with a 225GeV pion beam at the CERN SPS. The silicon beam telescope [19] provided the reference tracks with a nominal resolution of  $4\mu\text{m}$ . The telescope detectors and the devices under test were readout with the CMS APV25 analogue front end, which has a shaping time of 50ns and was synchronised to the 40MHz system clock. Non irradiated [20, 21] and irradiated up to  $2 \times 10^{15} n_{eq}/\text{cm}^2$  [22, 23] sensors were studied.

When summing the signals of two adjacent channels to avoid charge sharing effects a uniform response to the pions was observed in the non irradiated detectors, except for the electrode positions where less charge is collected. The overall efficiency, measured for a threshold of 1fC (this is the used by the binary readout of the ATLAS SCT), is  $(97.9 \pm 0.3)\%$ . The signal obtained from the irradiated devices is less uniform, larger in a thin region around the junction columns where the electric field is higher.

The values of the collected charge are very similar to the obtained in the laboratory tests from section 3.2. The non-irradiated 3D strip detector shows full collection from 50V. The irradiated 3D detectors show strong charge multiplication from sensor biases higher than 150V. For instance, at 230V the charge collected by the sensor irradiated to  $2 \times 10^{15} n_{eq}/\text{cm}^2$  is 31000 electrons, 136% of the non-irradiated signal (compare with Fig.3). This charge multiplication occurs mainly in the high electric field areas close to the collecting electrodes.

The signal-to-noise (S/N) ratio of the sensors was also calculated. The test beam had a large common mode noise that could not be reduced completely so the noise had to be measured separately in the laboratory with the Alibava system. The values of the S/N as a function of the applied bias for the detector irradiated to  $2 \times 10^{15} n_{eq}/\text{cm}^2$  are shown in Fig.4. The charge multiplication effect is beneficial for the signal-to-noise ratio for moderate voltages and values  $> 40$  can be achieved. However, at sensor biases  $> 230\text{V}$  the rapidly increasing noise makes the S/N ratio drop. The same behaviour at high biases is also seen in the detector irradiated to  $10^{15} n_{eq}/\text{cm}^2$  [23]. A better criterion to evaluate the detector performance for binary systems such as the ATLAS SCT, the signal-to-threshold ratio, is currently being investigated.

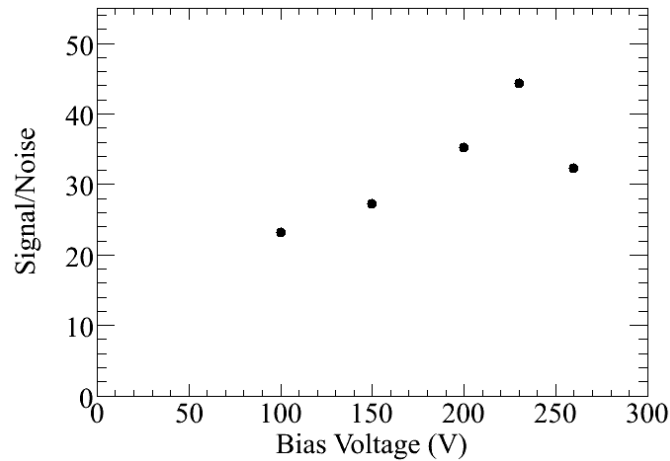


**Figure 4:** Signal-to-noise ratio of a 3D strip detector irradiated to  $2 \times 10^{15} n_{eq}/cm^2$  [22].

#### 4. Results from 3D Medipix2 detectors

This section focuses on results obtained with double-sided 3D pixel detectors compatible with the Medipix2, a photon-counting chip for hybrid pixel detectors developed for X-ray detection [24]. Medipix2 uses two discriminators to set an energy window, so a hit is accepted only if the signal is between two adjustable thresholds (only the lower energy threshold was used in our experiments.) The Timepix version of the chip can be operated in time over threshold mode, where a counter is incremented continuously as long as the signal is above threshold to give the energy deposited in the detector by the incident particle [25].

The 3D Medipix2 detectors were designed to be geometrically compatible with the Medipix2 readout chip and consist of an array of  $256 \times 256$  square pixels with an area of  $55 \times 55 \mu m^2$ . Each pixel is delimited by four biasing columnar electrodes in the back; in the centre of the pixel there is a collecting electrode. The active area of the sensor is surrounded by a ring of columns with the same doping type that the collection electrodes connected by a metal line to form a single guard ring. A 3D Medipix2 sensor fabricated on p-type silicon has the structure shown in Figure 1; if the substrate is n-type the column signs are the opposite.

The Medipix2 sensors were bump-bonded to Medipix2 readout chips and mounted on chip-boards. The boards were programmed and read out using the USB interface produced by IEAP, Czech Technical University, Prague [26].

##### 4.1 X-ray tests of Medipix2 detectors

3D Medipix2 detectors with n-type substrate were tested with X-rays at the Diamond Light Source, a third generation synchrotron located in Oxfordshire, UK. Tests of the response spectrum and Line Spread Function performed with a monochromatic X-ray beam in the energy range 12–20keV showed the lower charge sharing of the 3D structure (24% of charge shared events) with respect to an equivalent standard planar sensor (40%). Additionally, a 3D detector was used to

image diffraction rings produced by a powdered silicon sample, demonstrating for the first time the use of 3D detectors in a standard synchrotron experiment [27].

In a later beam test at Diamond [28, 29], 3D Medipix2 sensors fabricated on both p- and n-type silicon substrates were tested with a micro-focused X-ray beam in order to study the detection efficiency and the uniformity of the response of the 3D structure. An n-type planar sensor with the same thickness was also tested for comparison with the 3D. The beam size was  $4.5\mu\text{m}$  in X and  $6.7\mu\text{m}$  in Y and its energy was 14.5keV. The detectors were placed perpendicularly to the beam and raster scanned relative to the beam in  $2.5\mu\text{m}$  steps and the count rate per pixel was registered for each beam position. The resulting count rates as a function of the beam position were plotted in 2-D pixel maps like those shown in Figure 5, that correspond to a planar and a 3D n-type sensor in full depletion and a low energy threshold of 50% of the X-ray energy. In the planar sensor there are reduced detection efficiency areas in the pixel boundaries as the charge generated by a photon incident in these regions will be shared between the neighbouring pixels and the energy collected by each of them will fall below the threshold so the photon will not be counted. In the 3D sensor the electric field lines run parallel to the surface and thus the charge sharing is lower than for the planar. In the corners of the 3D sensor there are two competing effects: a reduction in the charge sharing thanks to the lateral electric field and a decrease in efficiency due to the presence of the columnar electrodes; both effects cancel out to give a similar efficiency than in the planar sensor. The reduction of the detection efficiency over the entire pixel due the collecting electrode located in the centre of the 3D pixel is 3% in the n-type detector and 4% in the p-type detector.

The characterization of the detection efficiency and charge sharing was performed at different bias voltages (lateral and full depletion in the case of the 3D sensor, in full depletion only for the planar sensor), and for three values of the lower threshold of the Medipix2 readout (25%, 50% and 75% of the X-ray beam energy.) The results confirm that the 3D sensors have a reduced under and over counting due to charge sharing than the equivalent planar pixel sensor, however there is an efficiency drop at the 3D electrodes and thus a non-uniform response across the pixel.

#### 4.2 Pion beam tests of Medipix2 detectors

The 3D Medipix2 pixel sensors were tested with a 225GeV pion beam at CERN with a telescope provided by the Medipix and the LHCb VELO upgrade communities. The telescope consists of six planar Medipix2 sensors and gives the position of the interaction of the individual pions with  $< 3\mu\text{m}$  accuracy. A discussion of the testbeam telescope is provided in [30]. The device under test was a double sided 3D n-type sensor bonded to a Timepix chip and operated in time over threshold mode.

The energy deposited by each particle was mapped as a function of the interaction point. For a pion interaction at zero angle, a drop in the signal can be observed at the electrode positions but there is full collection in the region between electrodes, similarly to the strip sensor tests from section 3.3. In the centre of the pixel only part of the charge deposited by the pions is collected due to the presence of the unfilled electrodes. In the pixel corners the same amount of charge is collected but this time the charge is shared between the four adjacent pixels [31].

The evolution of the collection efficiency with the angle was also studied as it is expected that avoiding particle tracks going through the entire columns improves the homogeneity of the response. The experimental results show that tilting the sensor by an angle between  $4^\circ$  and  $10^\circ$  the

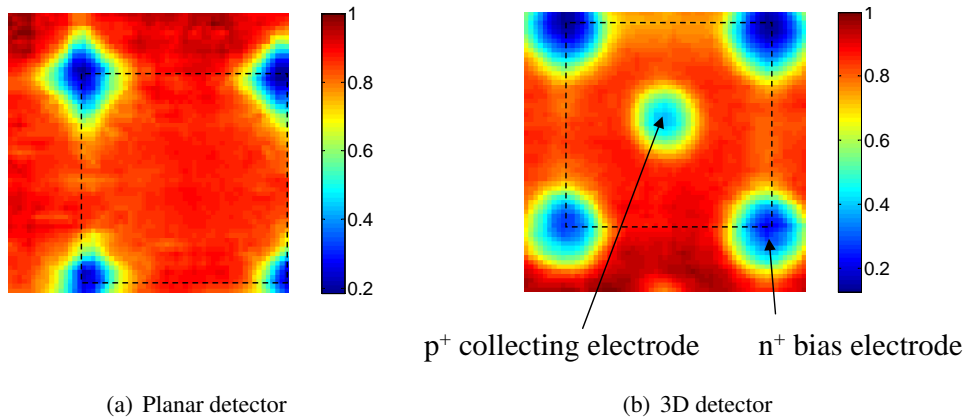


**Figure 5:** Pixel maps for a planar (a) and a 3D detector (b) fabricated on n-type silicon. The dashed squares indicate the edges of the pixel. The sensors are fully depleted and the lower threshold of the Medipix2 readout is 50% of the beam energy. The background has been subtracted and the count rates interpolated and normalized to the highest count.

collection inefficiency in the corners and centre disappears and the signal becomes homogeneous across the sensor. Similar results have been obtained by the 3D-ATLAS collaboration with 3D pixel detectors with passing-through columns and the ATLAS FEI3 readout [32].

## 5. Conclusions

There is clear evidence of charge multiplication in heavily irradiated 3D strip sensors obtained both in laboratory and beam tests. The signal-to-noise ratio of the sensors can be increased with the applied voltage up to a certain point, but it decreases again with very strong multiplication as the noise increases. This charge multiplication effect could be used to improve the performance of irradiated 3D detectors, but it is still not well understood and more experiments and simulations are needed at this point.

3D pixel detectors with Medipix2 readout show less charge sharing than the planar equivalent. The detection efficiency is not homogeneous within the detector and a reduced charge collection has been observed in the column regions due to charge loss inside the electrodes. However as the detector is rotated with respect to the incident beam the signal equalises across the detector and the inhomogeneities in efficiency disappear at an angle of less than  $10^\circ$ .

3D radiation detectors have shown to be a very promising solution for applications that require good radiation hardness or low charge sharing for improved spatial and spectral resolution. The double-sided 3D technology is already mature and ready for a small-medium scale production.

## Acknowledgments

This work has been partially supported by the Spanish Ministry of Education and Science through the GICSERV program "Access to ICTS integrated nano- and microelectronics cleanroom"

and by the Spanish CICYT project FPA2009-13896-C02-02. Part of this work was carried out in the context of the CERN RD50 and LHCb collaborations.

The authors would like to thank the Medipix collaboration for their support, the Karlsruhe Institute of Technology for the device irradiations and the personnel at Diamond Light Source for their invaluable help with the synchrotron studies.

The results shown in section 4.2 were produced in the context of a joint Medipix and LHCb testbeam, and we are indebted to the large team that contributed.

## References

- [1] S.I. Parker et al., *Nucl. Instr. and Meth. A*, **395** (1997) 328.
- [2] C. Da Vià et al., *IEEE Trans. Nucl. Sci.*, **56** (2009) 505.
- [3] A. Kok et al., these proceedings.
- [4] C. Kenney et al., *IEEE Trans. Nucl. Sci.*, **46** (1999) 1224.
- [5] T.-E. Hansen et al., *Journal of Instrumentation*, **4** (2009) P03010.
- [6] S. Ronchin et al., *Nucl. Instr. and Meth. A*, **573** (2007) 224.
- [7] G. Pellegrini et al., *Nucl. Instr. and Meth. A*, **592** (2008) 38.
- [8] A. Zoboli et al., *IEEE Trans. Nucl. Sci.*, **55** (2008) 2775.
- [9] D. Pennicard et al., *IEEE Trans. Nucl. Sci.*, **54** (2007) 1435.
- [10] D. Pennicard et al., *Nucl. Instr. and Meth. A*, **598** (2009) 67.
- [11] G. Lindström et al., *Nucl. Instr. and Meth. A*, **466** (2001) 308.
- [12] R.L. Bates et al., *2009 IEEE Nuclear Science Symposium Conference Record*, (2009) 148.
- [13] R. Marco-Hernández, *IEEE Trans. Nucl. Sci.*, **56** (2009) 1642.
- [14] A. Affolder et al., *Nucl. Instr. and Meth. A* (2010), doi:10.1016/j.nima.2010.02.187.
- [15] A. Zoboli et al., *2008 IEEE Nuclear Science Symposium Conference Record*, (2008) 2721.
- [16] I. Mandić et al., *Nucl. Instr. and Meth. A*, **603** (2009) 263.
- [17] G. Casse et al., these proceedings.
- [18] G. Casse et al., *Nucl. Instr. and Meth. A* (2010), doi:10.1016/j.nima.2010.04.085.
- [19] T. Mäenpää et al., *Nucl. Instr. and Meth. A*, **593** (2008) 523.
- [20] M. Köhler et al., in proceedings of *RD09*, PoS(RD09)031.
- [21] M. Köhler et al., *IEEE Trans. Nucl. Sci.* (2010), doi:10.1109/TNS.2010.2058863.
- [22] M. Köhler et al., presented at the *12th Topical Seminar on Innovative Particle and Radiation Detectors (IPRD10)*, 7–10 June 2010, Siena, Italy, to be published in *Nuclear Physics B (Proc. Suppl.)*.
- [23] M. Köhler et al., presented at *16th RD50 Workshop on Radiation hard semiconductor devices for very high luminosity colliders*, 31 May–02 June 2010, Barcelona, Spain, available from <http://indico.cern.ch/conferenceDisplay.py?confId=86625>.

- [24] X. Llopart et al., *IEEE Trans. Nucl. Sci.*, **49** (2002) 2279.
- [25] X. Llopart et al., *Nucl. Instr. and Meth. A*, **581** (2007) 485.
- [26] Z. Vykydal et al., *Nucl. Instr. and Meth. A*, **563** (2006) 112.
- [27] D. Pennicard et al., *IEEE Trans. Nucl. Sci.*, **57** (2010) 387.
- [28] A. Mac Raighne et al., *2009 IEEE Nuclear Science Symposium Conference Record*, (2009) 2145.
- [29] E.N. Gimenez et al., *Nucl. Instr. and Meth. A* (2010), doi:10.1016/j.nima.2010.06.140.
- [30] R. Plackett et al., these proceedings.
- [31] G. Stewart et al., presented at *The 5th Trento Workshop on Advanced Silicon Radiation Detectors, 24–26 February 2010, Manchester, UK*, available from <http://agenda.hep.manchester.ac.uk/conferenceTimeTable.py?confId=1181>.
- [32] H. Gjersdal et al., *Nucl. Instr. and Meth. A* (2010), doi:10.1016/j.nima.2010.04.083.